Science of the Total Environment 616–617 (2018) 1174–1180

Contents lists available at ScienceDirect

Science of the Total Environment

journal homepage: www.elsevier.com/locate/scitotenv

Under which climate and soil conditions the plant productivity–precipitation relationship is linear or nonlinear?

Jian-Sheng Ye *, Jiu-Ying Pei, Chao Fang

State Key Laboratory of Grassland Agro-ecosystems, School of Life Sciences, Key Laboratory for Semi-Arid Climate Change of the Ministry of Education, Lanzhou University, No. 222, South Tianshui Road, Lanzhou 730000, China

HIGHLIGHTS

- Nonlinear and linear pixels show similar precipitation variability.
- Nonlinear and linear pixels display similar extreme precipitation.
- Nonlinear pixels feature lower interannual NPP variability.
- Nonlinear pixels possess lower radiation and/or less soil nutrients.

GRAPHICAL ABSTRACT

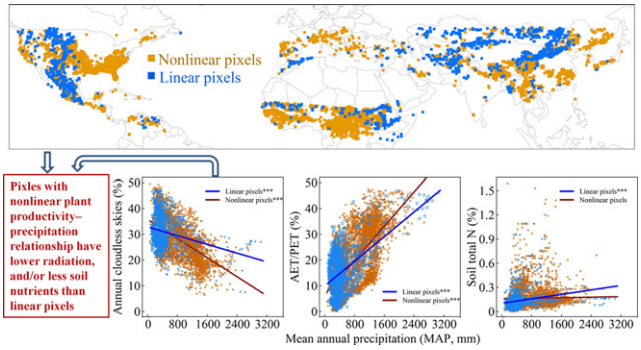
Nonlinear pixels
Linear pixels
Pixles with nonlinear plant productivity–precipitation relationship have lower radiation, and/or less soil nutrients than linear pixels
Annual cloudless skies (%)
AET/PET (%)
Soil total N (%)
Mean annual precipitation (MAP, mm)

ARTICLE INFO

Article history:
Received 11 September 2017
Received in revised form 19 October 2017
Accepted 20 October 2017
Available online 27 October 2017

Editor: Elena Paoletti

Keywords:
Climate change
Change in precipitation
Extreme precipitation
Remote sensing
Biomes
Terrestrial ecosystems

ABSTRACT

Understanding under which climate and soil conditions the plant productivity–precipitation relationship is linear or nonlinear is useful for accurately predicting the response of ecosystem function to global environmental change. Using long-term (2000–2016) net primary productivity (NPP)–precipitation datasets derived from satellite observations, we identify >5600 pixels in the North Hemisphere landmass that fit either linear or nonlinear temporal NPP–precipitation relationships. Differences in climate (precipitation, radiation, ratio of actual to potential evapotranspiration, temperature) and soil factors (nitrogen, phosphorous, organic carbon, field capacity) between the linear and nonlinear types are evaluated. Our analysis shows that both linear and nonlinear types exhibit similar interannual precipitation variabilities and occurrences of extreme precipitation. Permutational multivariate analysis of variance suggests that linear and nonlinear types differ significantly regarding to radiation, ratio of actual to potential evapotranspiration, and soil factors. The nonlinear type possesses lower radiation and/or less soil nutrients than the linear type, thereby suggesting that nonlinear type features higher degree of limitation from resources other than precipitation. This study suggests several factors limiting the responses of plant productivity to changes in precipitation, thus causing nonlinear NPP–precipitation pattern. Precipitation manipulation and modeling experiments should combine with changes in other climate and soil factors to better predict the response of plant productivity under future climate.

© 2017 Elsevier B.V. All rights reserved.

1. Introduction

Precipitation or alternatively water availability limits or co-limits plant production over almost all terrestrial ecosystems (Huxman et al.,

* Corresponding author.
E-mail address: yejiansheng30@gmail.com (J.-S. Ye).

https://doi.org/10.1016/j.scitotenv.2017.10.203
0048-9697/© 2017 Elsevier B.V. All rights reserved.

2004; Knapp et al., 2017). An intensification of temporal variability in precipitation is one of the most consistent changes that are being observed currently (Fischer and Knutti, 2016; Ye, 2014) and predicted for the future by global climate models (Easterling et al., 2000; IPCC, 2013). Net primary productivity (NPP) may respond linearly or nonlinearly to temporal changes in annual precipitation (PPT) (Hsu and Adler, 2014; Knapp et al., 2017). Thus, the mechanisms through which ecosystems NPP respond to PPT should be analysed to predict the biosphere feedback to climate systems characterised by strong interannual PPT variability (Huxman et al., 2004; Luo et al., 2017).

This study employs two NPP–PPT relationships: *spatial models* derived from NPP data of multiple ecosystems across a mean annual precipitation (MAP) gradient, and *temporal models* based on interannual NPP changes in response to variations in annual PPT for individual ecosystems (Estiarte et al., 2016; Huxman et al., 2004; Knapp et al., 2017; Ye et al., 2014). On a broad spatial scale, spatial models are usually nonlinear that NPP linearly increases with precipitation in its low range and levels off in high precipitation range (Estiarte et al., 2016; Huxman et al., 2004; Knapp et al., 2017; Ye et al., 2014). Temporal models are mostly found linear (Huxman et al., 2004; Knapp et al., 2017) and in some studies nonlinear (Hsu and Adler, 2014; Hsu et al., 2012). Knapp et al. (2017) suggest that with increasing interannual PPT variability and extreme PPT years under future climate, productivity may respond differently in extreme years than in nominal precipitation years, resulting in nonlinear response patterns. Under a climate with intensified interannual PPT variability, the nonlinear temporal NPP–PPT model will almost certainly better predict the response of NPP to change in PPT (Knapp et al., 2017). Spatially, the linear model better predicts NPP–PPT relationships during the driest years across ecosystems (i.e. when precipitation is the most limiting factor in each ecosystem), while the nonlinear model may exhibit high detection performance when resources other than precipitation become limited (Huxman et al., 2004).

We hypothesise that compared with linear ecosystems, nonlinear ones are characterised by (i) higher interannual precipitation variability (measured as coefficient of variation [CV]) and more occurrence of extreme precipitation years, and (ii) higher degree of limitation from climate and soil nutrient resources other than precipitation. Precipitation variability and extreme precipitation years increased in recent decades (Fischer and Knutti, 2016; Wang et al., 2010; Ye, 2014; Ye et al., 2017), which might provide opportunity to test these hypotheses. To test the two hypotheses on a large spatial scale, we divide terrestrial ecosystems in the North Hemisphere into two types i.e. ecosystems with either linear or nonlinear NPP–PPT relationships. We evaluate the difference between the two ecosystem types in terms of their climate and soil factors including PPT variability, radiation level, water deficit, contents of soil nitrogen (N), phosphorous (P), organic carbon (OC) and soil field capacity; these parameters and their interactions are important because they constrain ecosystem productivity (Hsu et al., 2012; Huxman et al., 2004; Seddon et al., 2016; Ye et al., 2013).

2. Materials and methods

2.1. Precipitation and net primary productivity

Precipitation and net primary productivity are two key variables used to analyse NPP–PPT relationships. Precipitation data are obtained from the Tropical Rainfall Measuring Mission (TRMM 3B43) satellite at 0.25° spatial resolution and monthly temporal resolution (TRMM, 2011). The dataset covers the latitude range of 50° N–S, and spans from January 2000 to December 2016 when our study was conducted. The 12-month rainfall rates are averaged to obtain the annual rates. TRMM rainfall rates are compared with high-quality observations of 1480 weather stations from the Global Historical Climatology Network (Menne et al., 2012). The TRMM rainfall data are consistent with precipitation observations of weather stations (Fig. S1).

Enhanced vegetation index (EVI) derived from the moderate-resolution imaging spectroradiometer (MODIS) sensor is used to estimate NPP. We use MOD13C2 version 6 product which provides monthly, global EVI at 0.05° resolution (Didan, 2015). Data collected from February 2000 to December 2016 are used in this study. EVI for January 2000 is estimated as the average of values in January of 2001–2005. When no clear-sky observations are available in some pixels, their corresponding data are excluded from our analysis. We also exclude pixels of water, croplands, urban and built-up, snow and ice, barren or sparse vegetation according to MODIS land cover type map (Channan et al., 2014). An offset of 0.05 is extracted from each monthly dataset to reduce the effects of soil exposure on EVI (Ponce Campos et al., 2013). The 12-month EVIs are integrated in TIMESAT software to obtain annually integrated EVI (iEVI, a proxy of NPP) for every pixel. The EVI data are integrated based on the default parameters used for TIMESAT initiation by using a previously reported method (Ponce Campos et al., 2013). Ponce Campos et al. (2013) found a linear relationship between the aboveground NPP (ANPP) and $iEVI^{1.15}$ at 10 sites across several biomes in US and Australia. To further validate the relation across all over the North Hemisphere, we compare iEVI and MODIS NPP (MOD17A3) (Running et al., 2004). We also find a similar linear relation (i.e. NPP is linearly related to $iEVI^{1.17}$) and thus confirm the robustness of such linear relationship (Fig. 1).

The algorithm of MOD17A3 MODIS NPP is based on radiation use efficiency (Running et al., 2004). The amount of absorbed photosynthetically active radiation translated to an actual productivity is determined by the conversion efficiency parameter, ε, which varies depending on vegetation types and climate conditions. The maximum ε is determined for each vegetation types and then multiplied by temperature and water–stress scalars to determine the gross primary productivity (GPP). MOD17A3 can also estimate the growth and maintain respiration, and the result is subtracted from the GPP to calculate NPP. Therefore, MOD17A3 NPP and iEVI apply different calculations. In this study, we use iEVI to evaluate the productivity–precipitation relationship because (i) the time series of MOD17A3 NPP dataset spans from 2000 to 2014, which is shorter than that of EVI; (ii) MOD17A3 NPP is calculated based on water availability and other climate variables, thus the dataset has an inherent productivity–precipitation relationship; and (iii) the calculation of iEVI is totally independent on climate and soil factors.

The plant growing season and peak EVI appear differently in the North and South Hemispheres. Only pixels in the North Hemisphere landmass (latitude range 0–50° N) are analysed in the present study for the convenience of integrating EVI values in TIMESAT and to use the longest available EVI and TRMM datasets (2000–2016). TRMM data are not available for 2017 when the study was conducted.

2.2. Climate and soil factors

Radiation (measured as mean annual average cloudless skies), water deficit (measured as ratio of actual to potential evapotranspiration), soil total N and P, SOC, soil field capacity (measured as volumetric water content [VMC] at −33 kPa) are obtained to analyse how these climate–soil factors constrain the response of NPP to changes in precipitation. All these factors and their interactions are considered to be important in limiting the ecosystem NPP (Fang et al., 2017; Hsu et al., 2012; Huxman et al., 2004; Seddon et al., 2016; Ye et al., 2013).

MODIS Cloud Mask products (MOD35_L2) are used as proxy for incoming radiation (Seemann et al., 2006). The proportion of clear sky to cloudy days in a given pixel can be derived from this product. The product shows good quality, except at approximately 60° N in northern Eurasia (Seddon et al., 2016). This does not influence our results because we limit the study region between 0 and 50° N latitudes. Water deficit or aridity is calculated as the ratio of actual evapotranspiration to potential evapotranspiration (AET/PET) (Seddon et al., 2016). AET and PET are obtained from the MOD16 Global Evapotranspiration products, which estimate AET and PET using the Penman–Monteith equation (Mu et

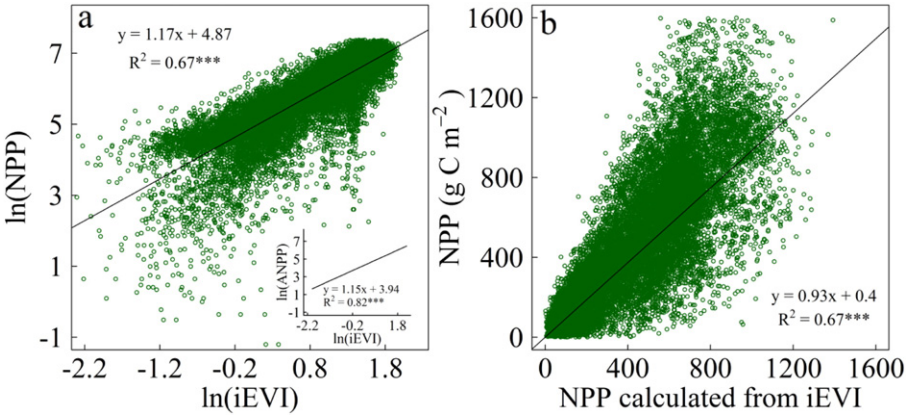

Fig. 1. Relationship between the MODIS net primary production (NPP) and annually integrated EVI (iEVI). We randomly select 1-year data during 2000–2016 to fit the log–log regression equation (a), and another 1-year data for validation (b). Significant codes for linear regressions: ***, $p < 0.001$. NPP is linearly related to $iEVI^{1.17}$, which is similar to the finding of Ponce Campos et al. (2013) that above-ground NPP (ANPP) is linearly related to $iEVI^{1.15}$ (inset of Fig. 1a). The slopes of our and Ponce Campos et al.'s log–log regression lines are not significantly different at $p = 0.05$, based on the procedure of Zar (2009). Ponce Campos et al. (2013) used above-ground NPP (ANPP) while MODIS NPP includes both above and below-ground NPP, thus the intercepts of the two regression lines are different. Since about 20000 pixels across the North Hemisphere are used to conduct the regression analysis, it is unlikely that all of them fit the regression line.

al., 2011). A lower ratio suggests higher water deficit or aridity. Mean annual averaged values of radiation and water deficit for the same period as NPP are calculated for each pixel. Temperature is a dominant factor limiting productivity in north of 50°N (Sun et al., 2016). Since high latitude regions are excluded from the current analysis, temperature is not considered as a limiting factor (Fig. S2).

Soil factors, including N, P, SOC and VWC, are obtained from the gridded Global Soil Dataset for use in Earth System Models (GSDE). GSDE provides soil properties include soil texture, organic carbon, and nutrients, which are quality controlled (Shangguan et al., 2014).

2.3. Data analysis

All the above iEVI, radiation, water deficit and soil data are resampled to 0.25° spatial resolution to match the low-resolution precipitation data of TRMM. For each pixel, the linear and nonlinear NPP–PPT relationships are determined by lm and nls functions in R Language. In this study, the linear temporal model is defined as NPP linearly increasing with precipitation, that is, positive slope (Estiarte et al., 2016; Huxman et al., 2004; Knapp et al., 2017; Ye et al., 2014). The nonlinear temporal NPP–PPT model is estimated by equation $NPP = a \times (1 - \exp(b \times PPT))$ (Huxman et al., 2004; Ye et al., 2014). We divide pixels of the North Hemisphere landmass into two types: (i) pixels that only fit the linear temporal NPP–PPT model (i.e. $p < 0.05$ for linear model and $p \geq 0.05$ for nonlinear model); (ii) pixels that only fit the nonlinear temporal NPP–PPT model (i.e. $p < 0.05$ for nonlinear model and $p \geq 0.05$ for linear model). To distinguish the two types, we exclude those that fit both linear and nonlinear models or fit neither linear nor nonlinear models for analysis.

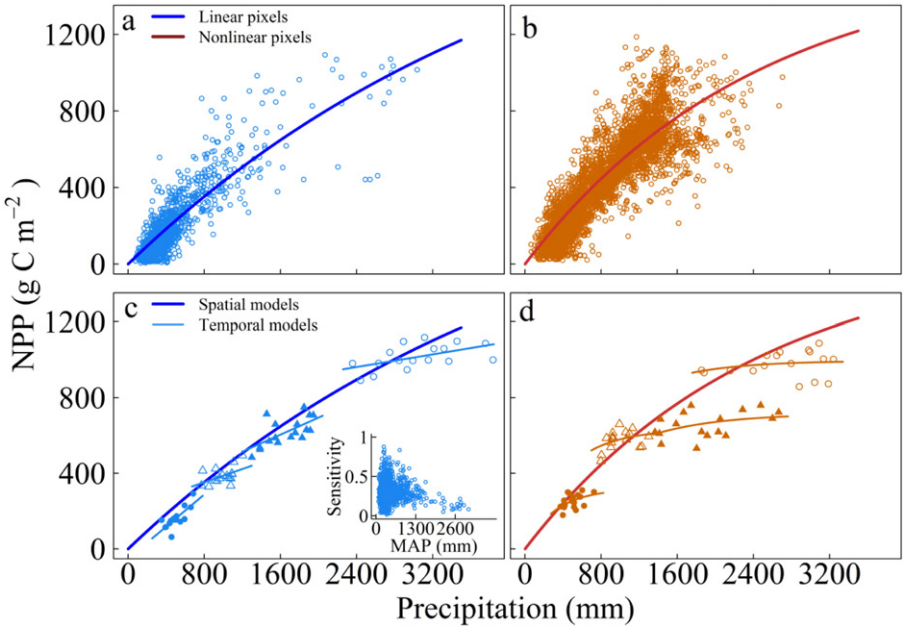

Fig. 2. Spatial and temporal relationships between net primary productivity (NPP) and precipitation. Pixels in the North Hemisphere are divided into two types i.e. pixels fit either linear or nonlinear temporal annual NPP–annual precipitation (PPT) relationships. (a) Spatial relationships of 17-year (2000–2016) mean NPP and mean annual precipitation (MAP) across 1497 linear pixels; the spatial model is $NPP = 2164 \times (1 - \exp(-0.0002 \times MAP))$, $p < 0.001$. (b) Same as (a) but across 4133 nonlinear pixels; the spatial model is $NPP = 1602 \times (1 - \exp(-0.0004 \times MAP))$, $p < 0.001$. (c) Temporal relationships of annual NPP–PPT during the 17-year are shown for selected linear pixels, and (d) nonlinear pixels. Inset shows the sensitivities of annual NPP to changes in annual PPT (i.e. slopes of the temporal NPP–PPT liner regressions) of the 1497 linear pixels.

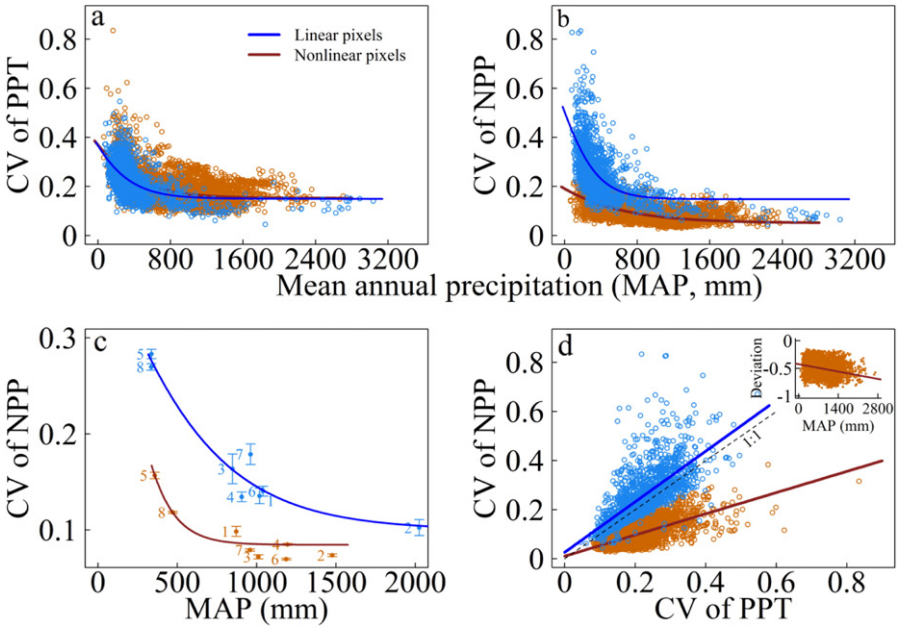

Fig. 3. Variabilities of interannual PPT and NPP during 2000–2016. (a) Interannual PPT variability (measured as coefficient of variation, CV), and (b) CV of NPP decrease with increasing mean annual precipitation (MAP) for both linear and nonlinear types; $p < 0.001$. (c) Biome–averaged CV of NPP decreases with increasing MAP for both linear and nonlinear types; 1 = evergreen needleleaf forest, 2 = evergreen broadleaf forest, 3 = deciduous broadleaf forest, 4 = mixture forest, 5 = open shurbland, 6 = woody savanna, 7 = savanna, 8 = grassland; error bar is one standard error; $p < 0.001$. (d) Relationships between CV of PPT and CV of NPP; linear pixels, $y = 1.03x + 0.03$, $p < 0.001$; nonlinear pixels, $y = 0.43x + 0.01$, $p < 0.001$; the slopes of the two regressions lines are significantly different at $p < 0.001$. Inset shows the deviation of the CV of NPP from that of PPT across the precipitation gradient for the nonlinear type; $y = -0.42 - 0.0001x$, $p < 0.001$.

To test the first hypothesis i.e. the nonlinear type has higher interannual precipitation variability and more occurrences of extreme precipitation years. We calculate the CV of PPT and occurrence of extreme precipitation years for each pixel based on the 17-year annual PPT data. Occurrences of extreme precipitation years are calculated using 'extremevalues' package in R Language https://www.github.com/markvanderloo/extremevalues. Briefly, the method uses a subset of the data to estimate the parameters for a model distribution by using regression of the sorted data on their quantile-quantile plot positions. A value in the dataset is considered as an extreme value when it is unlikely to be drawn from the estimated distribution. For our annual PPT data, the detected extreme is considered as extreme PPT that is unlikely to be drawn from the nominal PPT distribution for each pixel.

To test the second hypothesis i.e. the nonlinear type has higher degree of limitation from climate and soil nutrient resources other than precipitation. We compare the difference between the two types in terms of climate and soil factors. Permutational multivariate analysis of variance (perMANOVA) is applied to determine whether the linear and nonlinear types differ significantly when all climate and soil factors are considered collectively. The perMANOVA is a non-parametric multivariate statistical method to test whether the centroids and dispersions of some groups (i.e. linear and nonlinear pixel types in this study) are equivalent. The test requires no assumption concerning the number of variables (or their distributions) in the groups (Anderson, 2001). To allow for the comparison of climate and soil factors with different units, each of the six factors are standardised for each pixel as $X_{i,s} = (X_{i,o} - \mu_o) / sd_o$. Where $X_{i,s}$ is the standardised value and $X_{i,o}$ is original value for pixel i; μ_o and sd_o are the mean value and standard deviation of all pixels, respectively. The standardised values of each climate and soil factors (each pixel has one value for each factor) are used in the perMANOVA ("vegan" package, R Language). If the perMANOVA suggests the linear and nonlinear types differ significantly when the six climate–soil factors considered collectedly, the differences in each of the six factors are then evaluated. The linear regressions between MAP and each of climate–soil factors are conducted for the linear and nonlinear types, respectively. The differences of the regression lines between the two types are examined based on the procedure of Zar (2009).

3. Results

From the 20000 tested pixels (0.25 × 0.25° per pixel) across the North Hemisphere landmass (Fig. 1), our regression analyses of NPP–PPT find 1497 pixels that fit the linear temporal model and 4133 pixels that fit the nonlinear temporal model. Both linear and nonlinear types contain various biomes, including evergreen needleaf and broadleaf forests, deciduous broadleaf forests, mixed forests, shrublands, savannas, and grasslands. The overall spatial models derived from both types are nonlinear (Fig. 2a,b). However, the saturation value of NPP (about 2200 g C m^{-2}) derived from the linear type is higher than that from the nonlinear type (about 1600 g C m^{-2}) (Fig. 2a,b). The sensitivities/slopes of spatial models are steeper than those of the temporal models

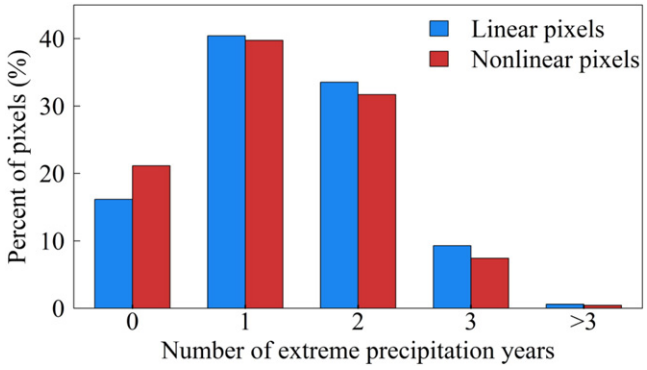

Fig. 4. The percentages of pixels detected with 0 to >3 extreme precipitation years during 2000–2016 for the linear and nonlinear types. Paired *t*-test suggests that the two types are not significant ($p = 0.94$).

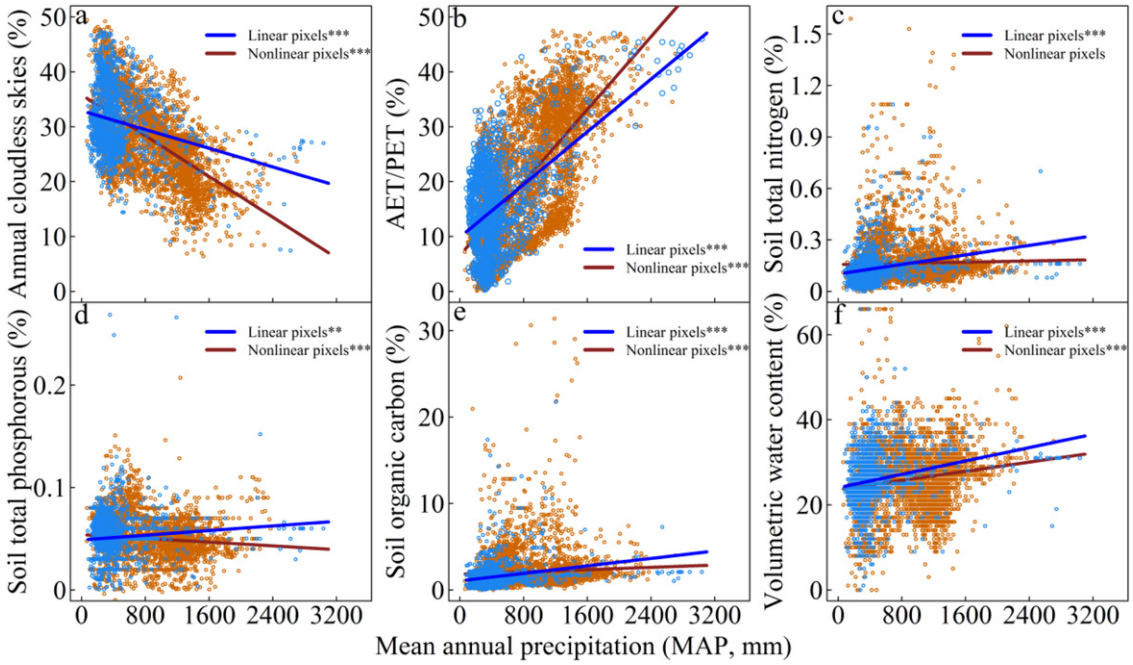

Fig. 5. Comparisons of six climate–soil factors between the linear and nonlinear types. The nonlinear type possesses lower cloudless skies (a), higher AET/PET (the ratio of actual to potential evapotranspiration) (b), lower soil total N content (c), P content (d), organic carbon content (e) and volumetric water content (f) in comparison with the linear type. Significant codes for linear regressions: ***, $p < 0.001$; **, $p < 0.01$; *, $p < 0.05$. Statistical differences in the slopes of linear regression lines between the two types are given in Table 1.

for both types (Fig. 2c,d), despite the same productivity–precipitation dataset between spatial and temporal models.

The CV of PPT decreases with increasing mean annual precipitation (MAP), and the patterns are similar between the linear and nonlinear types (Fig. 3a). The CV of NPP also decreases with increasing MAP for both types (Fig. 3b,c). However, the variabilities are higher in the linear type than that in the nonlinear type (Fig. 3b,c). The CV of PPT and CV of NPP are identical for the majority of the linear type pixels (the regression line is close to 1:1, Fig. 3d). By contrast, the CV of NPP is lower than CV of PPT in the nonlinear type; such deviation increases with increasing MAP (inset of Fig. 3d). To further test whether the nonlinear type has more extreme precipitation years than the linear type, the occurrences of extreme precipitation years in the two types are compared (Fig. 4). In the linear type, 84% pixels are found to have ≥1 extreme precipitation years during the study period of 2000–2016. The nonlinear type has 79% pixels with ≥1 extreme precipitation years, which is not significantly different from the linear type ($p = 0.94$).

Since the two types do not differ in interannual precipitation variability and occurrence of extreme precipitation years, we further evaluate differences in other environmental factors. The perMANOVA suggests that the two types differ significantly when the six climate (cloudless sky, AET/PET) and soil factors (TN, TP, SOC, and VMC) are considered collectively ($F = 131$, $p < 0.001$). Compared with the linear type, annual cloudless sky is lower and decreases faster with increasing MAP in the nonlinear type (Fig. 5a and Table 1). Nonlinear pixels mainly locate in east of USA, most of Europe, the Congo Basin, east of China, and Japan; these regions exhibit high limitation of sunlight (Fig. 6). Some of the nonlinear pixels are also distributed in region of high cloudless sky e.g. southern Europe (southern Spain and Portugal), this region is characterised by low soil nutrients (Fig. S3). The AET/PET is higher and increases faster with increasing MAP in nonlinear type than those in the linear type (Fig. 5b and Table 1). The soil contents of N, P and SOC and VMC are all lower in the nonlinear type than in the linear type (Fig. 5c–f). All soil factors increase with increasing MAP in the linear type. SOC and VMC also increase with increasing MAP in the nonlinear type, however, the slopes are significantly lower than those of the linear type (Fig. 5e,f and Table 1). By contrast, soil N does not change and soil P decreases with increasing MAP in the nonlinear type (Fig. 5c,d and Table 1). C/N and C/P ratios, indicators of N and P availabilities, increase with MAP in both linear and nonlinear types (Fig. S4).

Table 1
Regression between mean annual precipitation (MAP) and climate–soil factors as shown in Fig. 5. Statistical difference in the slopes of regression lines between the linear and nonlinear pixel types are compared based on the procedure of Zar (2009).

Factors[a]	Linear type pixels	Nonlinear type pixels	Slopes difference
Cloudless	$y = -0.004MAP + 33$ $p < 0.001$	$y = -0.009MAP + 36$ $p < 0.001$	$p < 0.001$
AET/PET	$y = 0.01MAP + 10$ $p < 0.001$	$y = 0.02MAP + 6$ $p < 0.001$	$p < 0.001$
TN	$y = 0.003MAP + 0.1$ $p < 0.001$	$y = 0.00001MAP + 0.2$ $p = 0.07$	$p < 0.001$
TP	$y = 0.00001MAP + 0.1$ $p < 0.01$	$y = -0.00001MAP + 0.1$ $p < 0.001$	$p < 0.001$
SOC	$y = 0.0007MAP + 1$ $p < 0.001$	$y = 0.0003MAP + 2$ $p < 0.001$	$p < 0.001$
VMC	$y = 0.004MAP + 2$ $p < 0.001$	$y = 0.003MAP + 2$ $p < 0.001$	$p < 0.05$

[a] Cloudless is annual cloudless skies (%); AET/PET is the ratio of actual to potential evapotranspiration (%); TN and TP are soil total nitrogen and phosphorous contents (%); SOC is soil organic carbon content (%); VMC is volumetric water content at −33 kPa (%), a proxy of soil field capacity.

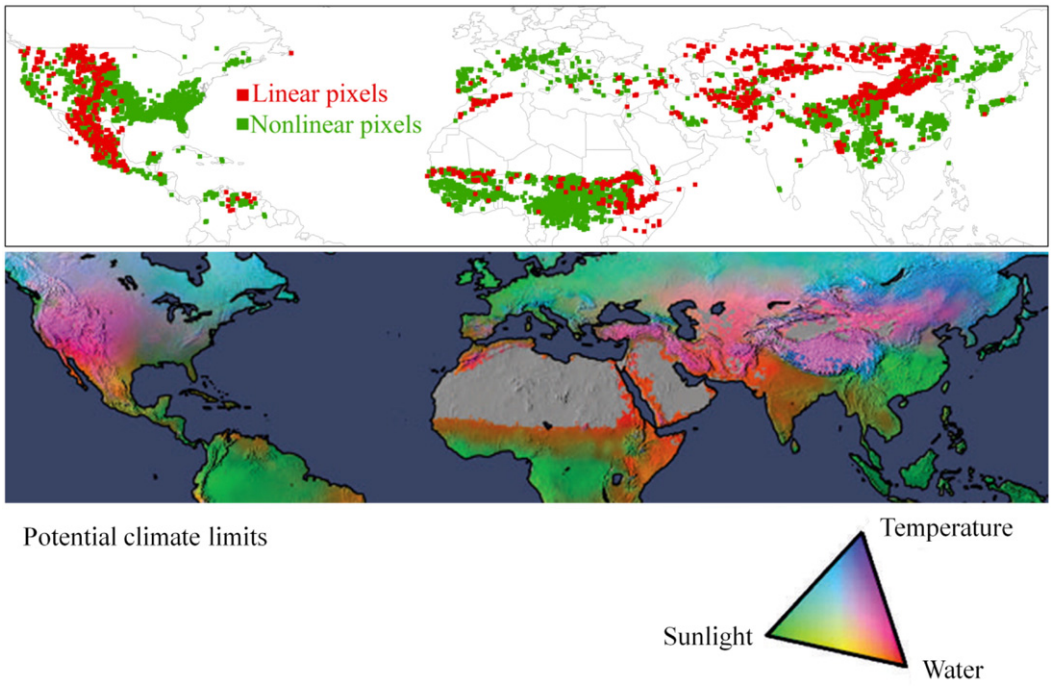

Fig. 6. Distributions of pixels with linear and nonlinear productivity–precipitation relationships in the North Hemisphere landmass (upper panel) and potential climate limits (lower panel, data from (Running et al., 2004)). Nonlinear pixels mainly locate in east of USA, most of Europe, the Congo Basin, east of China, and Japan. These regions exhibit high limits of sunlight.

4. Discussion

Based on NPP and precipitation derived from satellite products, we identify two types of temporal productivity–precipitation relationships (i.e. either linear or nonlinear) and evaluate the difference in climate and soil factors between them. Both types display nonlinear spatial NPP–PPT models across pixels, although they saturate in different precipitation regimes (Fig. 2a,b). The reduced responses of NPP to PPT in high precipitation ranges are probably due to increased limitation from radiation (measured by annual cloudless sky) and/or available soil nutrients, because these are the main limiting factors in high rainfall biomes such as tropical forests (Seddon et al., 2016). We also find two additional types of temporal NPP–PPT relationships i.e. pixels that fit neither linear nor nonlinear or fit both linear and nonlinear models. Pixels that have no relation with precipitation might be disturbed by human activities or other factors. For example, extreme precipitation events, instead of annual total precipitation, can also significantly influence NPP (Ye et al., 2016). Pixels that fit both linear and nonlinear models might be limited by both precipitation and other climate–soil factors.

Our findings do not support the hypothesis that nonlinear type is characterised by higher interannual PPT variability because both linear and nonlinear types possess similar interannual variability of PPT. Wilcox et al. (2017) propose that the nonlinear saturating form of NPP–PPT relationship is likely driven by less responses of NPP as extreme precipitation increases. We also compare the occurrences of extreme precipitation years between the linear and nonlinear types, and find no significant differences (Fig. 4). Thus, our findings do not support the suggestion that extreme precipitation is a direct driver of the nonlinear NPP–PPT relationship. However, we do not reject the prediction of Knapp et al. (2017) that the nonlinear temporal NPP–PPT model better predicts the response of NPP to PPT change for future climate conditions with increased interannual PPT variability and extreme PPT years. This prediction should be true if changes in PPT lead to other factors instead of precipitation becoming limited. Our analysis shows that the nonlinear type features higher sunlight deficit and lower water deficit, and/or less soil nutrients (N and P) and lower soil field capacity (measured by VMC) than the linear type (Fig. 5). Thus, the result supports the hypothesis that the nonlinear type has higher degree of limitation by resources other than precipitation. Low water deficit (measured by AET/PET) in the nonlinear ecosystem type results in low sensitivity of NPP to PPT changes because water is not the limiting factor. Low soil field capacity might lead to low available soil water because of high loss of precipitation via runoff or percolation especially during large rain events.

Our large-scale analysis suggests that the variability of NPP increased with increasing variability of PPT for both linear and nonlinear types; the results are consistent with previous findings (Fang et al., 2001; Ye et al., 2013). Moreover, NPP variability is generally equal to PPT variability in the linear type but deviates (negatively) from the latter in the nonlinear type (Anderson, 2001; Hsu and Adler, 2014; Hsu et al., 2012). Such negative deviations are larger in high MAP regions than in low MAP ones (inset of Fig. 3d), which might be due to reduction of radiation and soil nutrient contents (e.g. P) with increasing MAP in the nonlinear type. Therefore, NPP variability might not be related to PPT variability (for example Knapp and Smith (2001)) when resources other than precipitation are limited.

We find multiple climate and soil factors that limit the sensitivity of productivity to changes in precipitation. With increasing interannual precipitation variability and extreme precipitation years under climate change, it is necessary to consider would the availability of other environmental factors be significantly affected by changes in precipitation and then indirectly influence NPP (Luo et al., 2017). Thus, precipitation manipulation experiments and model simulation should combine with changes in other climate (such as radiation) and soil (such as N and P contents) factors to better predict the response of terrestrial ecosystem productivity.

Acknowledgements

This work is supported by the National Natural Science Foundation of China (grant numbers 31570467, 31770480), the project of State Key Laboratory of Grassland Agro-ecosystems of Lanzhou University

(grant number SKLGAE201705). We are grateful to the two anonymous reviewers for their in-depth comments and suggestion.

Appendix A. Supplementary data

Supplementary data to this article can be found online at https://doi.org/10.1016/j.scitotenv.2017.10.203.

References

Anderson, M.J., 2001. A new method for non-parametric multivariate analysis of variance. Austral Ecol. 26, 32–46.

Channan, S., Collins, K., Emanuel, W.R., 2014. Global Mosaics of the Standard MODIS Land Cover Type Data. University of Maryland and the Pacific Northwest National Laboratory, College Park, Maryland, USA.

Didan, K., 2015. MYD13C2 MODIS/Aqua Vegetation Indices Monthly L3 Global 0.05Deg CMG V006. NASA EOSDIS Land Processes DAAC.

Easterling, D.R., Meehl, G.A., Parmesan, C., Changnon, S.A., Karl, T.R., Mearns, L.O., 2000. Climate extremes: observations, modeling, and impacts. Science 289, 2068–2074.

Estiarte, M., Vicca, S., Peñuelas, J., Bahn, M., Beier, C., Emmett, B.A., et al., 2016. Few multiyear precipitation–reduction experiments find a shift in the productivity–precipitation relationship. Glob. Chang. Biol. 22, 2570–2581.

Fang, J., Piao, S., Tang, Z., Peng, C., Ji, W., 2001. Interannual variability in net primary production and precipitation. Science 293, 1723.

Fang, C., Ye, J.-s., Gong, Y., Pei, J., Yuan, Z., Xie, C., et al., 2017. Seasonal responses of soil respiration to warming and nitrogen addition in a semi-arid alfalfa-pasture of the Loess Plateau, China. Sci. Total Environ. 590, 729–738.

Fischer, E.M., Knutti, R., 2016. Observed heavy precipitation increase confirms theory and early models. Nat. Clim. Chang. 6, 986–991.

Hsu, J.S., Adler, P.B., 2014. Anticipating changes in variability of grassland production due to increases in interannual precipitation variability. Ecosphere 5, 1–15.

Hsu, J.S., Powell, J., Adler, P.B., 2012. Sensitivity of mean annual primary production to precipitation. Glob. Chang. Biol. 18, 2246–2255.

Huxman, T.E., Smith, M.D., Fay, P.A., Knapp, A.K., Shaw, M.R., Loik, M.E., et al., 2004. Convergence across biomes to a common rain-use efficiency. Nature 429, 651–654.

IPCC, 2013. Summary for policymakers. In: Stocker, T.F., Qin, D., Plattner, G.-K., Tignor, M., Allen, S.K., Boschung, J., et al. (Eds.), Climate Change 2013: The Physical Science Basis. Contribution of Working Group I to the Fifth Assessment Report of the Intergovernmental Panel on Climate Change. Cambridge University Press, Cambridge, United Kingdom and New York, NY, USA, pp. 1–30.

Knapp, A.K., Smith, M.D., 2001. Variation among biomes in temporal dynamics of aboveground primary production. Science 291, 481–484.

Knapp, A.K., Ciais, P., Smith, M.D., 2017. Reconciling inconsistencies in precipitation–productivity relationships: implications for climate change. New Phytol. 214, 41–47.

Luo, Y., Jiang, L., Niu, S., Zhou, X., 2017. Nonlinear responses of land ecosystems to variation in precipitation. New Phytol. 214, 5–7.

Menne, M.J., Durre, I., Vose, R.S., Gleason, B.E., Houston, T.G., 2012. An overview of the global historical climatology network-daily database. J. Atmos. Ocean. Technol. 29, 897–910.

Mu, Q., Zhao, M., Running, S.W., 2011. Improvements to a MODIS global terrestrial evapotranspiration algorithm. Remote Sens. Environ. 115, 1781–1800.

Ponce Campos, G.E., Moran, M.S., Huete, A., Zhang, Y., Bresloff, C., Huxman, T.E., et al., 2013. Ecosystem resilience despite large-scale altered hydroclimatic conditions. Nature 494, 349–352.

Running, S.W., Nemani, R.R., Heinsch, F.A., Zhao, M., Reeves, M., Hashimoto, H., 2004. A continuous satellite-derived measure of global terrestrial primary production. Bioscience 54, 547–560.

Seddon, A.W.R., Macias-Fauria, M., Long, P.R., Benz, D., Willis, K.J., 2016. Sensitivity of global terrestrial ecosystems to climate variability. Nature 531, 229–232.

Seemann, S.W., Borbas, E.E., Li, J., Menzel, W.P., Gumley, L.E., 2006. MODIS Atmospheric Profile Retrieval Algorithm Theoretical Basis Document, Version 6.

Shangguan, W., Dai, Y., Duan, Q., Liu, B., Yuan, H., 2014. A global soil data set for earth system modeling. J. Adv. Model. Earth Syst. 6, 249–263.

Sun, Y., Piao, S., Huang, M., Ciais, P., Zeng, Z., Cheng, L., et al., 2016. Global patterns and climate drivers of water-use efficiency in terrestrial ecosystems deduced from satellite-based datasets and carbon cycle models. Glob. Ecol. Biogeogr. 25, 311–323.

TRMM, 2011. TRMM (TMPA) Rainfall Estimate L3 3 hour 0.25 degree × 0.25 degree V7. Goddard Earth Sciences Data and Information Services Center (GES DISC), Greenbelt, MD.

Wang, H., Fu, R., Kumar, A., Li, W., 2010. Intensification of summer rainfall variability in the Southeastern United States during recent decades. J. Hydrometeorol. 11, 1007–1018.

Wilcox, K.R., Shi, Z., Gherardi, L.A., Lemoine, N.P., Koerner, S.E., Hoover, D.L., et al., 2017. Asymmetric responses of primary productivity to precipitation extremes: a synthesis of grassland precipitation manipulation experiments. Glob. Chang. Biol. 1–10.

Ye, J.-S., 2014. Trend and variability of China's summer precipitation during 1955–2008. Int. J. Climatol. 34, 559–566.

Ye, J.-S., Reynolds, J.F., Sun, G.J., Li, F.M., 2013. Impacts of increased variability in precipitation and air temperature on net primary productivity of the Tibetan Plateau: a modeling analysis. Clim. Chang. 119, 321–332.

Ye, J.-S., Reynolds, J.F., Li, F.-M., 2014. A mechanistic-bioclimatic modeling analysis of the potential impact of climate change on biomes of the Tibetan Plateau. Ecology 95, 2109–2120.

Ye, J.-S., Reynolds, J.F., Maestre, F.T., Li, F.-M., 2016. Hydrological and ecological responses of ecosystems to extreme precipitation regimes: a test of empirical-based hypotheses with an ecosystem model. Perspect. Plant Ecol. 22, 36–46.

Ye, J.-S., Gong, Y.-H., Zhang, F., Ren, J., Bai, X.-K., Zheng, Y., 2017. Which temperature and precipitation extremes best explain the variation of warm vs. cold years and wet vs. dry years? J. Clim. https://doi.org/10.1175/JCLI-D-17-0377.1 (in press).

Zar, J.H., 2009. Biostatistical Analysis. Fifth Edition. Prentice Hall, Upper Saddle River, NJ.